Fractality and the law of the wall

Haosen H. A. Xu and X. I. A. Yang

Phys. Rev. E **97**, 053110 — Published 29 May 2018

DOI: 10.1103/PhysRevE.97.053110

Fractality and the law of the wall

X. I. A. Yang[1,2] and Haosen H. A. Xu[1]
[1]Mechanical and Nuclear Engineering, Penn State University, Pennsylvania, 16801
[2]Center for Turbulence Research, Stanford University, Stanford, CA, USA, 94305

Fluid motions in the inertial range of isotropic turbulence are fractal, with their space-filling capacity slightly below regular three-dimensional objects, which is a consequence of the energy cascade. Besides the energy cascade, the other often encountered cascading process is the momentum cascade in wall-bounded flows. Despite the long-existing analogy between the two processes, many of the thoroughly-investigated aspects of the energy cascade have so far received little attention in studies of the momentum counterpart— e.g., the possibility of the momentum-transferring scales in the logarithmic region being fractal has not been considered. In this work, this possibility is pursued, and we discuss one of its implications. Following the same dimensional arguments that lead to the $D = 2.33$ fractal dimension of wrinkled surfaces in isotropic turbulence, we show that the large-scale momentum-carrying eddies may also be fractal and non-space-filling, which then leads to the power-law scaling of the mean velocity profile. The logarithmic law of the wall, on the other hand, corresponds to space-filling eddies, as suggested by A. A. Townsend. Because the space-filling capacity is an integral geometric quantity, the analysis presented in this work provides us with a low-order quantity, with which, one would be able to distinguish between the logarithmic law and the power law.

I. INTRODUCTION

A visually striking feature of turbulence is that it is intermittent, with regions of vigorous fluid motions among regions that are quiescent. Being spatially intermittent, turbulence and turbulent eddies are not necessarily space-filling [1]. After the pioneering work of Kolmogorov in 1962 [2], it is commonly acknowledged that eddies in the inertial range are fractal, with their space-filling capacity slightly below regular 3D objects [3]. The flow intermittency and the resulting fractality are often modeled using the fractal [4] and multi-fractal models [5], and such work dates back to Ref. [6], where isotropic turbulence (HIT) was modeled as a hierarchy of self-similar eddies. Eddies being fractal in the inertial range has implications on a number of flow processes. The process of interest here is the turbulent transport process. Figure 1 sketches such a transporting process. The transported quantity ϕ has a finite difference across the self-similar wrinkled interface. Statistically, coarse-graining this surface at scales l_L, l_S within the inertial range yields similar flow structures. The coarse-grained turbulent flux $F(l)$ can be modeled as

$$F(l) = \nu_{T,l} \frac{d\phi_l}{dl} S(l), \tag{1}$$

where $\nu_{T,l}$ is the eddy viscosity at the coarse-graining length scale l, $d\phi_l/dl$ is the gradient of the coarse-grained quantity ϕ_l at the scale l, and $S(l)$ is the surface area of the wrinkled interface at the scale l [3, 7–9]. In the inertial range, dimension arguments suggest $\nu_{T,l} \sim \langle\epsilon\rangle^{1/3} l^{4/3}$ and $d\phi_l/dl \sim \Delta\phi/l$, where $\langle\epsilon\rangle$ is the mean dissipation rate. The turbulent flux, $F(l)$, is a conserved physical quantity and cannot depend on the coarse-graining length scale l, therefore it follows from Eq. (1) that $S(l) \sim l^{-1/3}$. The area of a fractal surface coarse-grained at a length scale l can be measured by box counting, where the area is $S(l) \sim N(l)l^2$, and $N(l) \sim l^{-D}$ is the number of intersecting boxes. The exponent D is the fractal dimension of S. In Eq. (1) $S(l) \sim l^{-1/3}$, it then follows that the space dimension of S is $D = 2 + 1/3 \approx 2.33$. (See Ref. [10] for detailed discussion on the above dimensional arguments.) The fractal scaling $D = 2.33$ may be tested by considering a turbulent-non-turbulent-interface (TNTI), which can be defined based on the vorticity magnitude [11], the turbulent intensity [9], etc.. A recent work [12] confirmed the power-law scaling of $S(l) \sim l^{2-D}$, and the measured $D \approx 2.31$ is not inconsistent with the fractal model.

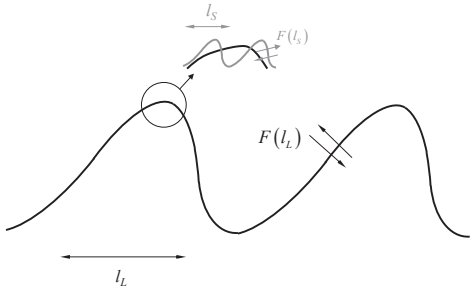

FIG. 1. A sketch of a coarse-grained wrinkled interface, across which a transported quantity ϕ has a finite difference $\Delta\phi$. The interface is self-similar across a range of scales $l_S < l < l_L$, where l_L and l_S are two coarse-graining length scales. Flow structures are statistically similar at the two coarse-graining length scales.

In the inertial range of HIT, the dominating process is the energy cascade from large-scale motions to small-scale motions. Turbulence is fractal as a result of this process (see detailed discussion in Ref. [4]). The other often encountered cascade process is the momentum cascade in wall-bounded flows [13]. While early investigations on the two cascade processes were rather indepen-

dent, recently there have been attempts to model the momentum cascade using tools that were developed for the energy cascade [14–17]. Nevertheless, analysis as the one in Eq. (1) has not been pursued in the context of wall-bounded flows, and we have not yet considered the possibility of momentum-carrying scales being fractal in wall-bounded flows. This work is to fill this gap.

II. FRACTALITY

A. Fractal formalism

At a wall-normal location $y \sim O(0.2\delta)$, the flow is not everywhere turbulent because of intrusions of non/less-turbulent fluid from the freestream/bulk [18, 19]. Turbulent transport of the streamwise momentum in the wall-normal direction is only possible in regions where there is active turbulence. Hence, momentum transport is not a space-filling process. To parameterize non-space-filling processes, one often uses a space whose dimension is below a regular object in the base dimension. Using the same dimensional arguments that lead to Eq. (1), we can model the momentum flux in the inertial range of wall-bounded flows (which is often referred to as the log region) as

$$F(y) = \nu_{T,y} \frac{dU}{dy} S(y), \tag{2}$$

where y is the wall-normal coordinate and U is the mean velocity. Momentum flux is constant in the log region, hence $F(y) \sim y^0$. Dimension arguments suggest that in the inertial range, $\nu_{T,y} \sim u_\tau y$ [20], where u_τ is the friction velocity, and is the only relevant velocity scale in the log region. dU/dy can be computed from the law of the wall. The two most often quoted mean-flow scalings are the logarithmic scaling [21, 22] and the power-law scaling [23, 24]. The log law reads as follows

$$U^+ = \frac{1}{\kappa} \log(y^+) + B, \tag{3}$$

where "log" is natural log, the superscript + indicates normalization by wall units, κ is the von Karman constant and B is an additive constant. According to the log law dU/dy is $\sim 1/y$, and it follows that $S(y) \sim$ Const is independent of the wall-normal distance. This is trivial, and simply means that the momentum-carrying eddies in the inertial range (log region) are space-filling [25]. On the other hand, the power law reads as follows

$$U^+ = C y^{+\alpha}, \tag{4}$$

where $C > 0$ and $\alpha < 1$ are constants that depend on the friction Reynolds number and flow configuration. For flows at moderate Reynolds numbers, $\alpha = 1/7$ is often quoted [26]. According to the power law, $dU/dy \sim y^{\alpha-1}$ and $S(y) \sim y^{-\alpha}$, and the momentum-carrying turbulence is fractal.

While it has long been acknowledged that the energy-transferring scales in the inertial range are fractal, the possibility of momentum-carrying eddies in wall-bounded flows being fractal has not been thoroughly explored, and the above analysis suggests that an implication of non-space-filling momentum-carrying eddies is the power-law scaling of the mean velocity profile. The analogy between the energy cascade and the momentum cascade was considered by Jimenez [13]. Because the energy cascade is from large scales to small scales and the momentum cascade is from the freestream to the wall (from the channel/pipe center-line to the wall), the analogy is between the coarse-graining length scale in the context of HIT and the wall-normal distance.

Considering the difference in the scaling of $S(y)$ when the mean flow follows a log scaling ($S(y) \sim y^0$) and a power-law scaling ($S(y) \sim y^{-\alpha}$), the space-filling capacity $S(y)$ may be used to discriminate between a power-law scaling and a log scaling. It is worth noting that discriminating between a log scaling and a power-law scaling is many times not straight-forward because both scalings provide good fits to the mean velocity in the near-wall region [27]. The difference between a log law and a power law is only evidenced when one considers dU/dy (where the log law leads to $ydU/dy \sim$ Const and the power law leads to $ydU/dy \sim y^\alpha$), but differentiating measurements that already suffer from experimental uncertainties can bring in errors that defy even the power-law scaling of dU/dy. The space-filling capacity $S(y)$ is therefore useful here—$S(y)$ is a low-order statistical quantity, and therefore its measurement is less susceptible to experimental uncertainties.

We still need to define $S(y)$. Before doing that, we briefly review the definition of the coarse-grained interface $S(l)$ in HIT. $S(l)$ in HIT is usually defined by thresholding a physical quantity. The commonly used quantities include the turbulent kinetic energy [12], the vorticity magnitude [11, 28], and the scalar concentration [10, 29]. Although not without trial and error, measurements of iso-surfaces of those quantities have yielded $D = 2.2$ to $D = 2.4$ for $S(l)$. For wall-bounded flows, because ϕ in Eq. (2) is the streamwise momentum U, $S(y)$ can be defined by thresholding the streamwise velocity fluctuation. In this work we formally define $S(y) = \int_{|u^+(x,y,z)-U^+(y)|>c} dx\, dz$, where u is the instantaneous streamwise velocity. This definition is to capture the momentum-transporting motion, i.e., the large scale and very large scale motions and the low-momentum streaks in the near-wall region [30, 31], where the velocities are far from the local mean values. However, thus defined $S(y)$ is affected by intrusions of the non-turbulent freestream [18]. Therefore we consider instead the complementary dimension and define

$$\mathcal{S}(y) = \int_{|u^+(x,y,z)-U^+(y)|<c} dx\, dz, \tag{5}$$

For $\mathcal{S}(y)$, the log law and the power law lead to $\mathcal{S}(y) \sim y^0$ and $\mathcal{S}(y) \sim y^\alpha$, respectively.

B. Internal flows and external flows

The above discussion does not discriminate between internal flows and external flows, and we have argued that fractality in wall-bounded turbulence is because of intrusions of the irrotational freestream, which presents only for external flows but not for internal flows. Internal flows including channel and pipe are often considered to be fully turbulent. However, according to a few recent works, the above physical picture may need to be revised slightly. Using channel flow data up to $Re_\tau = 4000$, Kwon et. al. [32] found a quiescent core in turbulent channel flow. The quiescent core has high velocity magnitude and low turbulence intensity, and it very much resembles the free stream of boundary layers. Hence there is good reason to believe that for this work we do not have to discriminate between internal and external flows.

While it might not be directly relevant to this work, the β- model [4] models HIT as a mixture of quiescent and turbulent flows despite the fact that HIT is often considered as being fully turbulent.

C. Fractal dimension, coarse-graining and wall-normal distance

The analogy between the energy cascade and the momentum cascade was thoroughly discussed in Ref. [11], and it follows that the coarse-graining length scale in the context HIT is analogous to the wall-normal distance in boundary-layer flows. Here we show that the filtered streamwise velocity at a wall-normal height corresponds to the unfiltered streamwise velocity at a higher height. We do that by resorting to the Townsend attached eddy hypothesis [25]. Townsend hypothesized that, at high Reynolds numbers, wall-bounded turbulence may be modeled as collections of wall-attached eddies (see figure 2 for a sketch). The velocity at a generic location in the flow field is the superposition of the eddy-induced velocities there. For example, the velocity fluctuation at the wall-normal height **C** contains incremental contributions from eddy-hierarchy I, eddy-hierarchy II, and eddy-hierarchy III, while the velocity fluctuation at the wall-normal height **A** contains incremental contribution from only eddy-hierarchy I. Because of the wall-attachment, the eddy population density is inversely proportional to the wall-normal distance y, i.e. $P(y) \sim 1/y$. If the wall-attached eddies are self-similar, the variance of the streamwise velocity is

$$\left\langle u'^2 \right\rangle \sim \int_y^\delta P(y)dy = \log(\delta/y), \tag{6}$$

which scaling has gained much empirical support [22, 27, 34, 35]. Here, u' is the streamwise velocity fluctuation, δ is an outer length scale and $\langle\cdot\rangle$ denotes ensemble averaging.

Here, we consider the scaling of $\left\langle u_l'^2 \right\rangle$, where u_l' is the filtered streamwise velocity fluctuation at a given wall-normal height, and l is the filtering length scale. For example, let us consider the scaling of $\left\langle u_l'^2 \right\rangle$ as a function of l at the wall-normal height **C**. According to the Townsend attached eddy hypothesis, the velocity fluctuation at the wall-normal height **C** bears footprints of eddy-hierarchy I, eddy-hierarchy II, and eddy-hierarchy III. Because the sizes of the eddies scale with their distances from the wall, contributions from eddy-hierarchy III are at comparably smaller scales than those from eddy-hierarchy I and II. Hence we may remove contributions from eddy hierarchy-III by applying a low-pass filter to the velocity fluctuations. After low-pass filtering the velocity fluctua-

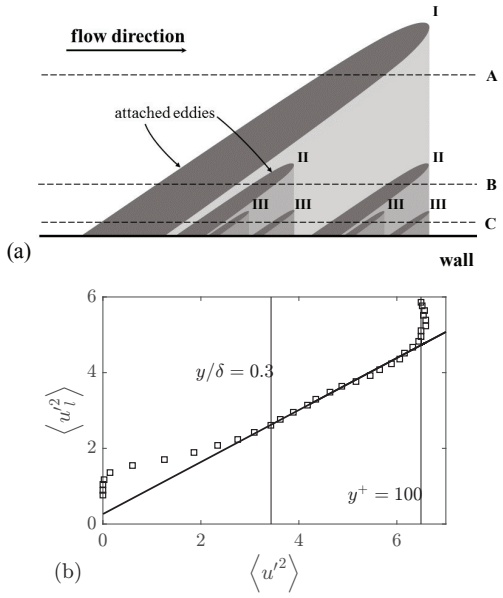

FIG. 2. (a) A sketch of the hypothesized wall-bounded turbulence at high Reynolds numbers. Three hierarchies of wall-attached eddies are sketched I, II, III. An eddy affects the flow within. The eddies are wall-attached, and are inclined towards the flow direction. The sizes of the eddies scale with their distance from the wall, and therefore the number of the eddies double as the size halves. Here, there are one hierarchy-I eddy, two hierarchy-II eddies, and four hierarchy-III eddies. **A**, **B** and **C** are at three wall normal heights. (b) Filtered streamwise velocity at $y^+ = 100$ as a function of the variance of the streamwise velocity fluctuation. $\left\langle u_l'^2 \right\rangle$ is a function of the filtering length scale l, and $\left\langle u'^2 \right\rangle$ is a function of the wall-normal distance y. By relating y and l, i.e., $z = l\tan(\theta)$, we can relate $\left\langle u_l'^2 \right\rangle$ to $\left\langle u'^2 \right\rangle$, which leads to the plot shown here. Here $\theta = 12^\circ$ is the inclination angle of a typical wall-attached eddy [33]. We have used the top-hat filter in Fourier space. While not shown, using a top-hat filter in physical space leads to similar results. The two thin solid lines are at $\left\langle u'^2 \right\rangle\Big|_{y=0.3\delta}$ and $\left\langle u'^2 \right\rangle\Big|_{y^+=100}$. The bold solid line indicates the proportionality between $\left\langle u_l'^2 \right\rangle$ and $\left\langle u'^2 \right\rangle$.

tion, $\left\langle u_l'^2 \right\rangle$ corresponds to $\left\langle u'^2 \right\rangle$ at a wall-normal height $y = l\tan(\theta)$, where $\theta \approx 12^\circ$ is the inclination angle of a typical wall-attached eddy [33]. If the attached eddies are self-similar,

$$\left\langle u_l'^2 \right\rangle \sim \left\langle u'^2 \right\rangle\Big|_{z=l\tan(\theta)}. \quad (7)$$

Figure 2 (b) shows $\left\langle u_l'^2 \right\rangle$ as a function of $\left\langle u'^2 \right\rangle$, and the expected proportionality is indeed found within $y^+ = 100$ and $y/\delta = 0.3$. Hence we have formally connected the wall-normal distance with a properly defined filtering length scale. It also follows from the discussion that what was observed through S is, strictly speaking, self-similarity.

Marusic and co-authors have also explored the relation between filtered velocity at one wall-normal height and the unfiltered velocity at a higher wall-normal height, and the reader is directed to Refs. [36, 37] for details.

D. Measurements

We analyze the hot-wire data of boundary layer flow at Re_τ=13,000 and measure $\mathcal{S}$(y) directly. The data were from the Melbourne High-Reynolds-Number-Boundary-Layer-Wind-Tunnel. The experiments were not conducted by the authors of the paper. As hot-wire data are one-dimensional, $\mathcal{S}(y)$ is simply $\int_{|u^+(x,y)-U^+(y)|<c} dx$. Details of the experimental facility and the hot-wire data can be found in Refs. [38, 39] and the references cited therein. In Ref. [39], one can also find details of measurements at lower Reynolds numbers.

Figure 3 (a) shows the measured $\mathcal{S}$ as a function of the wall-normal distance. We have used $c = 2$. $\mathcal{S}$ is roughly a constant within $50 < y^+$, $y^+ < C_y\sqrt{Re_\tau}$, where $C_y \approx 4.4$, and it follows a power law in the region $0.1 < y/\delta$, $y/\delta < 0.3$. Intrusions of freestream/quiescent-core to the viscous boundary layer are expectedly weak in the near-wall region where viscous effects are not negligible, and therefore the fractal to space-filling transition location is expectedly at the wall-normal location where the viscous effects are negligible above this location. Wei et al. [40] considered the balance of terms in the mean momentum equation and showed that viscous effects are non-negligible up to $y^+ \sim \sqrt{Re_\tau}$, which conclusion was later confirmed in Refs. [41, 42]. Following these works and the works by Mckeon & Sharma [43] and Marusic et. al. [22], here we scale the fractal-space-filling transition location with the $y^+ \sim \sqrt{Re_\tau}$. According to the analysis in section II A, the mean flow follows a log scaling in the region $50 < y^+$, $y^+ < C_y\sqrt{Re_\tau}$, and a power-law scaling in the region $0.1\delta < y$, $y < 0.3\delta$, with an power-law exponent $\alpha = 0.13$. Figure 3 (b) shows the corresponding mean velocity as a function of the wall-normal distance. The log scaling in Fig. 3 (b) is the best fit for U in the region where $\mathcal{S} \sim y^0$, and the resulting von Karman constant is $\kappa = 0.39$. The power law is the best fit for U in the region where $\mathcal{S} \sim y^{0.13}$, and the resulting power-law exponent is indeed $\alpha = 0.13$, confirming the fractal model. Throughout this work, we keep only two significant digits for all the log-law and power-law parameters. We make a few observations. First, the mean velocity follows the power-law scaling in the region $C_y\sqrt{Re_\tau} < y^+$, $y/\delta < 0.3$. Second, the log law can be used as the law of the wall in the region $30 < y^+$, $y/\delta < 0.1$ [44]. Third, both the log and the power-law scalings may be used for U in the intermediate wall-normal distance range $C_y\sqrt{Re_\tau} < y^+$, $y/\delta < 0.1$.

The momentum-transferring scales being non-space-filling is possibly because of intrusions of non/less-turbulent flows from the freestream/bulk [18]. The significance of freestream intrusion increases as y/δ increases, and the momentum-carrying scales are fractal away from the wall. At a wall-normal distance where y/δ is not sufficiently close to 0 and y^+ is not sufficiently large, the flow may be at an intermittent state, where it is space-filling sometimes and non-space-filling the other times. Because the presence of the logarithmic scaling relies on the flow being space-filling at all times and the presence of the power-law scaling relies on the flow being non-space-filling at all times, in principle, neither the logarithmic scaling nor the power-law scaling may be used for approximating the mean velocity profile within the intermediate wall-normal range. The data, however, shows that both scalings may be used.

In Fig. 3 (a), we have set $c = 2$. $\mathcal{S}$ depends on the threshold c and fluctuations from non-momentum-transferring motions (small-scale intermittency). The fractal model in section II A is further tested in Fig. 4 by using a different threshold and by filtering the velocity signals. The same y^0 and $y^{0.13}$ scalings survive when using a c that changes the measured $\mathcal{S}$ by $\approx 40\%$. No noticeable changes are found in $\mathcal{S}$ when the hot-wire signals are filtered using a top-hat filter that spans $\Delta x^+ \approx 100$ (this is to preclude the small scales).

We also test the usefulness of the fractal formalism at low and moderate Reynolds numbers. Figure 4 (b) shows $\mathcal{S}(y)$ in a $Re_\tau \approx 5200$ channel. Details of this dataset can be found in Ref. [35]. DNS provides the full 3D flow field, and $\mathcal{S}(y)$ can be measured using data on $x-z$ planes. Nonetheless, as the flow field is homogeneous in the spanwise direction, measuring $\mathcal{S}(y)$ using data on the $x-z$ planes is not different from measuring $\mathcal{S}(y)$ using one-dimensional hot-wire data [45]. At a moderate Reynolds number, neither the y^0 scaling nor the y^α scaling can be found. Therefore the analysis in §II A is really only useful at high Reynolds numbers. Following the discussion in the previous section, this is because, at moderate Reynolds numbers, there is not a wall-normal location where y/δ is sufficiently close to 0 and y^+ is sufficiently large simultaneously, and fluid across the entire boundary layer is at the intermediate state where it is sometimes space-filling and other times non-space-filling.

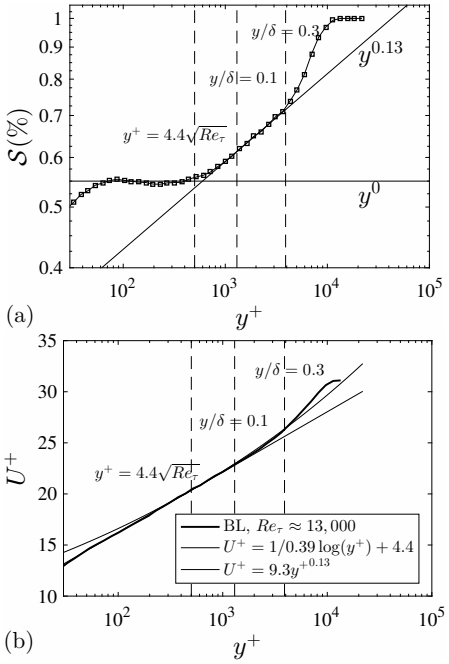

FIG. 3. (a) The measured $\mathcal{S}(y)$ as a function of the wall-normal distance on a log-log scale. We have normalized $\mathcal{S}(y)$ using the length of the signal. The two solid lines indicate $\sim y^0$ and $\sim y^{0.13}$, respectively. The dashed lines are at wall normal distances $y^+ = C_y\sqrt{Re_\tau}$, $y/\delta = 0.1$ and $y/\delta = 0.3$, respectively, where $C_y = 4.4$. (b) The mean velocity (bold line) as a function of the wall-normal distance on a semi-log scale. The constants in the log scaling and in the power-law scaling are $\kappa = 0.39$, $B = 4.4$, and $C = 9.7$, $\alpha = 0.13$.

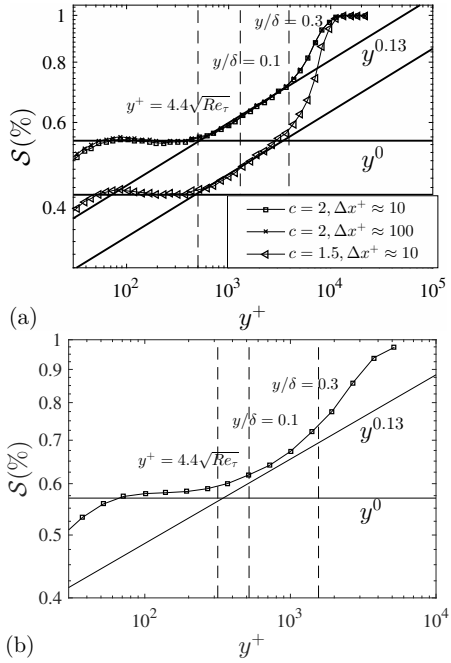

FIG. 4. (a) Measured $\mathcal{S}(y)$ as functions of the wall-normal distance. $c = 1.5$ and $c = 2$ are used. Δx is the filtering length scale. The resolution of the hot-wire data is $\Delta x^+ \approx 10$ (assuming a constant convective velocity $U_c = 0.8U_\infty$, and invoking the Taylor's frozen turbulence hypothesis. U_∞ is the free-stream velocity). (b) $\mathcal{S}(y)$ in a DNS channel at $Re_\tau = 5200$ [35]. $c = 2$ is used.

III. THE LAW OF THE WALL

The mean flow behavior in wall-bounded turbulence has received sustained attention over the past few decades [46, 47]. Although other mean-flow scalings may be found in the literature [40, 48], the most often quoted scalings are the log law and the power law.

A. Dimension arguments

Both the log law and the power law can be derived using just dimension arguments. We briefly summarize these arguments and discuss how the analysis in section II may be incorporated. We start by considering a range of wall normal distances where u_τ is the only relevant velocity scale. Dimension arguments suggest

$$\frac{dU}{dy} \sim \frac{u_\tau}{y} f\left(y^+, \frac{y}{\delta}\right), \tag{8}$$

where $u_\tau = \sqrt{\tau_w/\rho}$, and τ_w equals the momentum flux in the inertial range, y^+, y/δ are the only two non-dimensional numbers that may be formed with the relevant length and velocity scales. For the log law, we take the limit $y^+ \to \infty$, $y/\delta \to 0$, and assume f is finite and non-zero at that limit. It then follows from Eq. (8) that $dU/dy \sim u_\tau/y$, which then leads directly to the log law. For the power law, on the other hand, one needs to argue that the a non-zero f at the limit $y^+ \to \infty$, $y/\delta \to 0$ does not exist, and $f(y^+, y/\delta)$ follows instead a power law in the near wall region (taking the leading order term). This then leads to $dU/dy \sim u_\tau/y^{1-\alpha}$, which in turn gives rise to the power law. The above dimensional analysis is incomplete. To make that clear, we quote the interesting argument by Kazakov (2016) [48], where the author took one step further and considered the scaling of dU^p/dy, which, according to the same dimension arguments, scales as u_τ^p/y. If f is finite at the limit $y^+ \to \infty$, $y/\delta \to 0$, Eq. (8) leads to $U \sim [\log(y^+)]^{1/p}$, instead of the log law.

To make the above dimension arguments complete, one needs to account for the fractality of the momentum-transferring eddies. Before we do that, we briefly summarize the dimension arguments Kolmogorov used for the 2/3 scaling in isotropic turbulence. In the inertial range, the two-point velocity increment Δu^2 scales as $(\epsilon l)^{2/3} g(l/(\nu^3/\epsilon)^{1/4}, l/L)$, where l is the two-point displacement, L is an integral length scale and g is a general function of $l/(\nu^3/\epsilon)^{1/4}$ and l/L. Kolmogorov [6] assumed that g is non-zero and finite at the limit $l/(\nu^3/\epsilon)^{1/4} \to \infty$, $l/L \to 0$ and obtained $\Delta u^2 \sim l^{2/3}$. Kolmogorov [6] then concluded that $\Delta u^p \sim (\epsilon l)^{p/3}$, which was later refuted by

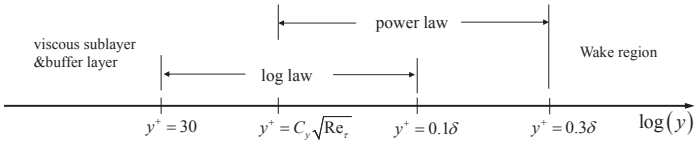

FIG. 5. A sketch of the wall layer.

experimental measurements. Although the existence of a non-zero finite g at the limit $l/(\nu^3/\epsilon)^{1/4} \to \infty$, $l/L \to 0$ was not formally proven, the flaw in Ref. [6], as Kolmogorov himself [2] later pointed out, is really in that it failed to account for the fact that turbulence is fractal in the inertial range in HIT. The complete dimension arguments for Δu^p accounts for the fractal dimension of turbulence, and is $\Delta u^p \sim (\epsilon l)^{p/3} \cdot (l/L)^{3-D_p}$, where $(l/L)^{3-D_p}$ is the fractal scaling. Hence the argument in Ref. [48] can be augmented by accounting for the fractal dimension.

Hence taking the limit $y^+ \to \infty$, $y/\delta \to 0$ in Eq. (8) is probably not problematic, but assuming the momentum cascade process in wall-bounded flows being a space-filling process is. As fractal dimension scalings are power-law scalings, the postulated $f \sim y^\alpha$ in the so-called incomplete similarity [49, 50] is really to account for the fractal scaling of turbulence in wall-bounded flows. Last, it is worth noting that dU^p/dy in wall-bounded flows scales as $u_\tau^p/y \cdot (y/\delta)^{2-D_p}$, where $(y/\delta)^{2-D_p}$ is to account for turbulence being fractal.

B. Law of the wall

In the above sections, we have provided both theoretical arguments and empirical evidence for the fractal nature of the momentum-carrying eddies in wall-bounded turbulence. Here we provide indirect evidence by examining the mean velocity profiles.

Conventionally, the extent of the log range is determined by first fitting a log scaling to a velocity profile and then using the fitted log scaling to determine the extent of the log range. The above procedure is based on a circular logic. Ideally, one needs to use a separate diagnostics for the extent of the log range, and then fit a log scaling to that range. The usefulness of the log scaling can then be tested by examining the quality of the fitting. This is where the analysis in section II becomes useful. The quantity $\mathcal{S}$ is a separate metric for determining the extent of the log-range/power-law-range. Following the discussion in the previous section, the following wall-layer composition in Fig. 5 will be tested using the data. The wall-layer composition in Fig. 5 is found to provide good working approximations of the velocity profiles in channel, pipe and boundary-layer flows (see appendix A). It is worth noting that the space-filling capacity of boundary layer turbulence was recently discussed in [18] and [51], albeit in different contexts.

Compared to the log law, the power law is less practical because of the Reynolds number dependence of the two power-law parameters. The analysis in section II may be used to provide estimates of the power-law parameters. From to Fig. 3 (a), we conclude that the transition from being space-filling to being non-space-filling is continuous. Therefore, the power-law parameters are in principle functions of the log-law parameters. Because both the power-law and the log-law can be used to approximate the mean velocity in the overlap region, the constants in the power law may be determined by fitting a power law scaling to a log scaling in the overlap region, i.e. C and α are such that e in the following equation is at its minimum

$$e = \int_{y^+=C_y\sqrt{Re_\tau}}^{y^+=0.1\delta^+} \left(\frac{1}{\kappa}\log(y^+) + B - Cy^{+\alpha}\right)^2 d\log(y^+). \quad (9)$$

This problem can be solved numerically, and both C and α are functions of κ and B. However, because this procedure relies on the existence of an overlap region ($0.1\delta^+ > C_y\sqrt{Re_\tau}$), it provides predictions only for flows at a friction Reynolds number $Re_\tau \gtrsim 2,000$. In Fig. 6, the predicted C and α are compared against the measurements. We have used $\kappa = 0.44$, $B = 6.2$ for pipe flow, $\kappa = 0.39$, $B = 4.2$ for boundary layer flow and $\kappa = 0.41$, $B = 5.2$ for channel flow (the constants κ and B for each flow are the averages among the cases of that flow configuration). As a result, the predicted C and α are different for pipe, boundary layer and channel. The empirical function in Ref. [52] is included for comparison. The predicted power law constants agree reasonably well with the measurements, and the current predictions are not very different from previous empirical functions, except for the dependency on κ and B. Hence the fractal analysis in Sect. II is further supported.

IV. CONCLUSIONS

A fractal model is developed for the momentum transfer process in wall-bounded flows. The presence of the logarithmic law relies on the momentum-transferring eddies being space-filling, and the power law corresponds to non-space-filling momentum-transferring scales. A low-order quantity, i.e., the space-filling capacity, is identified that allows us to probe directly the derivative of the mean velocity. Data analysis of this low-order quantity shows that log scaling provides a reasonably good fit for the mean velocity profile in the region $30 < y^+$, $y < 0.1\delta$ and the power law fits the mean velocity quite well in $C_y\sqrt{Re_\tau} < y^+$, $y < 0.3\delta$, where $C_y \approx 4.4$. The region $C_y\sqrt{Re_\tau} < y^+$, $y/\delta < 0.1$ is an overlap region, where the flow transitions from a space-filling state to a non-space-filling state. The dimension arguments that lead to the log law and the power law are also revisited, and we discuss how the fractal scaling may be incorporated in conventional dimension arguments.

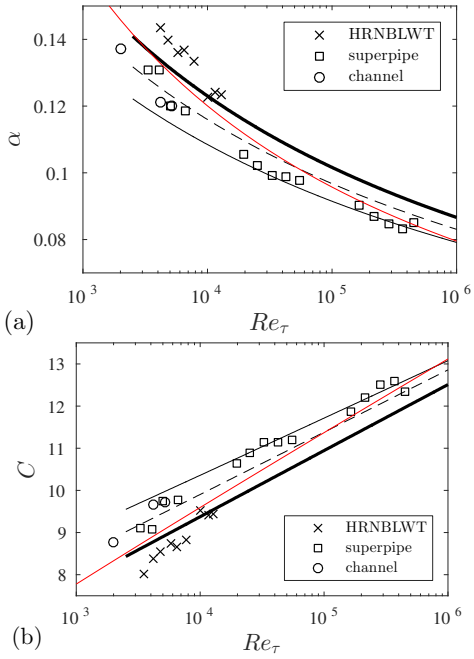

FIG. 6. (a) power law exponents and (b) prefactor as functions of the friction Reynolds number. Symbols are measurements, and are best fits of power-law scalings to U in the wall-normal distance range $0.1 < y/\delta < 0.3$, within which region $\mathcal{S}(y)$ follows a power-law. The bold line, thin line and the dashed line correspond to Eq. (9) for boundary layer, pipe and channel, respectively. The thin red line in (a) corresponds to the empirical correlation by [52]: $\alpha = 1.085/\log(Re) + 6.535/(\log(Re))^2$, where Re is the bulk Reynolds number, and is defined based on the pipe diameter and the flow rate. The bulk Reynolds number Re can be related to the friction Reynolds number Re_τ using the Karman-Prandtl resistance relation, i.e., $1/\sqrt{f} = -1.930\log(1.90/(Re\sqrt{f}))$, where $f = 8\tau_w/(\rho\bar{U}^2)$, and $\bar{U}$ is the mean flow rate. The thin red line in (b) corresponds to $C = 0.7053\log(Re) + 0.3055$ [52].

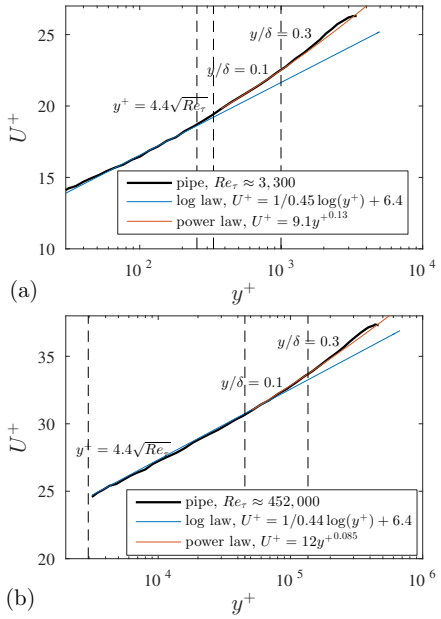

FIG. 7. Mean velocities as functions of the wall-normal distance for pipe flow at (a) $Re_\tau \approx 3,300$ and (b) $Re_\tau \approx 452,000$ on a semilog scale. Legends are the same as in Fig. 3 (b).

The discussion on the asymptotic regime within which a universal law of the wall can be expected is likely to continue [53–55], so as theoretical and modeling investigations on possible functional forms of the law of the wall [40, 56–63]. We do not attempt to conclude these discussions in this work. Neither have we discussed important issues such as the universality of the von Karman constant [64, 65], nor the implication of the present work on rough wall boundary layer flows [66–68]. This work is only to provide a new perspective to the historical research topic of the law of the wall, and we hope a few new insights can be gained by making an analogy between the energy cascade and the momentum cascade.

Appendix A: Empirical evidence

We use experimental data from the Princeton superpipe [49, 69], the Melbourne HRNBLWT [39] and DNS data in Refs. [35, 70–73]. The constants κ, B in the log law and C, α in the power law are allowed to vary from case to case. For most datasets, a log scaling is fitted in the region $50 < y^+ < C_y\sqrt{Re_\tau}$, within which region, $\mathcal{S}(y)$ is independent of the wall-normal distance. For high Reynolds number datasets (e.g. the $Re_\tau \approx 452,000$ dataset), where the first off-wall measuring wire is at a wall-normal height $y^+ > C_y\sqrt{Re_\tau}$, we fit a log scaling in the wall-normal range between the first off-wall measuring height and $y/\delta = 0.05$. For low Reynolds number datasets, where $C_y\sqrt{Re_\tau} > 0.1\delta^+$, we fit a log scaling in the region $50 < y^+$, $y/\delta < 0.1$. The power law is fitted in the region $0.1 < y/\delta < 0.3$, within which region $\mathcal{S}(y)$ follows a power law. Similar exercise has been done in the literature. Here we do not seek to repeat those analyses. As we have discussed, the extents of both the log scaling and the power-law scaling are determined using a separate measure $\mathcal{S}(y)$, and in this section, we test first the usefulness of the two scalings in the respective region and second the fractal model .

Figure 7 shows the pipe flow results. For brevity, we show only data at a moderate Reynolds number, i.e., $Re_\tau \approx 3,300$, and data at a high Reynolds number, i.e., $Re_\tau \approx 452,000$. For the $Re_\tau \approx 3,300$ case, the mean flow follows the power law scaling from $y^+ \approx 30$ to $y/\delta \approx 0.5$. For the $Re_\tau \approx 452,000$ case, the mean profile follows the fitted power law scaling from the first off-wall measuring height, which is slightly above $y^+ = C_y\sqrt{Re_\tau}$, to $y/\delta = 0.5$. Both the power law and the log law provide good fits to the mean flow in the wall distance range $C_y\sqrt{Re_\tau} < y^+$, $y/\delta < 0.1$. Figure 8 shows the channel flow results. For brevity, we show only data at two Reynolds numbers, i.e. $Re_\tau \approx 1,000$ [73] and

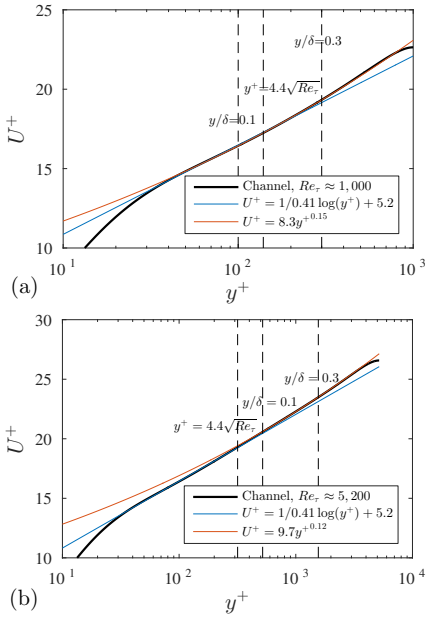

FIG. 8. Mean velocities as functions of the wall-normal distance for channel flow at (a) $Re_\tau \approx 1,000$ and (b) $Re_\tau \approx 5,200$ on a log-linear scale. Legends are the same as in Fig. 3 (b).

$Re_\tau \approx 5,200$ [35]. The log scaling provides a reasonably good fit for the mean velocity up to $y/\delta \approx 0.15$ at both Reynolds numbers. The power law scaling, on the other hand, is a good fit for the mean flow in the region $y/\delta \approx 0.1$ to $y/\delta \approx 0.3$. For channel and pipe flow, where the fluid is forced by a favorable pressure gradient, the mean velocity profile is only slightly above the power law in the wake region. In Fig. 3 (b), we have already shown the $Re_\tau \approx 13,000$ boundary layer results. In Fig. 9, we show the results for boundary layer at $Re_\tau \approx 4,800$. The log scaling deviates from the mean profile at $y/\delta \approx 0.1$. The mean velocity profile follows the power-law scaling in the region $100 < y^+$, $y/\delta < 0.3$. Hence the fractal model is supported by the data—logarithmic scaling provides a good fit for the mean velocity near the wall, and the in the bulk region the mean profile follows a power law. The extents of the log and power-law regions predicted by the fractal model are, however, conservative. Near the wall, the flow becomes space-filling, and the transition from non-space-filling to space-filling is in the wall-normal extent $C_y\sqrt{Re_\tau} < y^+$, $y/\delta < 0.1$. In addition, comparing Fig. 9, Fig. 3 (b) with Fig. 7, Fig. 8, one may have preferred the power law over the log law for pipe and channel flow [74], and preferred the log law over the power law for boundary layer flow [22].

Both the von Karman constant κ and the addend B in the log law depend on the friction Reynolds number and the flow configuration, e.g. $\kappa \approx 0.38$ to 0.40 in boundary layer flow, $\kappa \approx 0.42$ to 0.44 in pipe flow, and $\kappa \approx 0.41$ in channel flow. Despite this variation, $\kappa \approx 0.4$ to a single digit. The multiplier C and power exponent α in the power law, on the other hand, depends more explicitly on the friction Reynolds number.

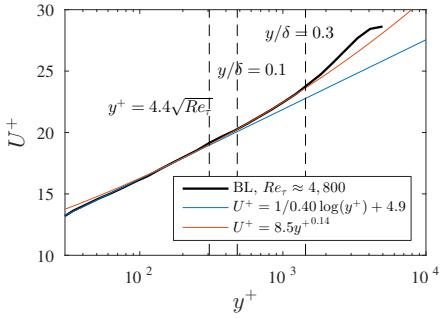

FIG. 9. Mean velocity as functions of the wall-normal distance for boundary layer flow at $Re_\tau \approx 4,800$ on a semi-log scale.

Appendix B: A remark on the wall-layer composition

Data analysis in section II D suggests that neither a log scaling nor a power-law scaling may be used for U in the overlap region ($C_y\sqrt{Re_\tau} < y^+$, $y/\delta < 0.1$), however, in this appendix A, the data suggest that both scalings can be used for U in the overlap region. At infinite Reynolds number, the overlap region spans an infinite number of scales and a log scaling is incompatible with a power law scaling, thus the law of wall as is in Fig. 5 is in principle not possible. Here we examine at what Reynolds number a power-law scaling can no longer be used to approximate a log scaling (and vice versa). The atmospheric boundary layer on Earth is at a friction Reynolds number $Re_\tau \approx O(10^6)$. Atmospheric boundary layers on other planets and stars may be at higher Reynolds numbers, but it is unlikely that we would be dealing with wall-bounded flows at friction Reynolds numbers $Re_\tau > 10^{20}$. At $Re_\tau = 10^{20}$ the overlap region extends more than eight decades of scales. The uncertainty in von Karman constant is ± 0.02, i.e. $\kappa = 0.38 \sim 0.42$. This uncertainty in κ is a $\pm 5\%$ uncertainty in the mean velocity. If we fit a power law scaling to a perfect logarithmic scaling $U^+ = 0.4\log(y^+) + 5.0$ in the overlap region. The fitted power law is well within the $\pm 5\%$ uncertainty. Hence we conclude that, for all practical purposes, the sketched wall layer in Fig. 5 can be used, and the mean velocity in the overlap region can be approximated using either the log law or the power law.

ACKNOWLEDGMENTS

The work is funded by the US AFOSR, Grant #1194592-1-TAAHO monitored by Dr. Ivett Leyva. XY would like to acknowledge P. Moin and C. Meneveau for their generous help.

[1] K R Sreenivasan, "Fractals and multifractals in fluid turbulence," Ann. Rev. Fluid Mech. **23**, 539–604 (1991).

[2] A N Kolmogorov, "A refinement of previous hypotheses concerning the local structure of turbulence in a viscous incompressible fluid at high Reynolds number," J. Fluid Mech. **13**, 82–85 (1962).

[3] K R Sreenivasan and C Meneveau, "The fractal facets of turbulence," J. Fluid Mech. **173**, 357–386 (1986).

[4] Uriel Frisch, Pierre-Louis Sulem, and Mark Nelkin, "A simple dynamical model of intermittent fully developed turbulence," J. Fluid Mech. **87**, 719–736 (1978).

[5] C Meneveau and K R Sreenivasan, "Simple multifractal cascade model for fully developed turbulence," Phys. Rev. Lett. **59**, 1424 (1987).

[6] Andrei N Kolmogorov, "The local structure of turbulence in incompressible viscous fluid for very large Reynolds numbers," Dokl. Akad. Nauk SSSR **30**, 301–305 (1941).

[7] C Meneveau and KR Sreenivasan, "The physics of chaos and systems far from equilibrium," Nucl. Phys , 49 (1987).

[8] Charles Meneveau and K R Sreenivasan, "Interface dimension in intermittent turbulence," Phys. Rev. A **41**, 2246 (1990).

[9] Jimmy Philip, Charles Meneveau, Charitha M de Silva, and Ivan Marusic, "Multiscale analysis of fluxes at the turbulent/non-turbulent interface in high Reynolds number boundary layers," Phys. Fluids **26**, 015105 (2014).

[10] K R Sreenivasan, R Ramshankar, and C Meneveau, "Mixing, entrainment and fractal dimensions of surfaces in turbulent flows," Proc. Roy. Soc. London Ser. A. **421**, 79–108 (1989).

[11] Javier Jiménez, Sergio Hoyas, Mark P Simens, and Yoshinori Mizuno, "Turbulent boundary layers and channels at moderate Reynolds numbers," J. Fluid Mech. **657**, 335–360 (2010).

[12] Charitha M de Silva, Jimmy Philip, Kapil Chauhan, Charles Meneveau, and Ivan Marusic, "Multiscale geometry and scaling of the turbulent-nonturbulent interface in high Reynolds number boundary layers," Phys. Rev. Lett. **111**, 044501 (2013).

[13] Javier Jiménez, "Cascades in wall-bounded turbulence," Ann. Rev. Fluid Mech. **44**, 27–45 (2012).

[14] X I A Yang, I Marusic, and C Meneveau, "Hierarchical random additive process and logarithmic scaling of generalized high order, two-point correlations in turbulent boundary layer flow," Phys. Rev. Fluids **1**, 024402 (2016).

[15] Xiang I A Yang, Ivan Marusic, and Charles Meneveau, "Moment generating functions and scaling laws in the inertial layer of turbulent wall-bounded flows," J. Fluid Mech. **791**, R2 (2016).

[16] Xiang I A Yang, Charles Meneveau, Ivan Marusic, and Luca Biferale, "Extended self-similarity in moment-generating-functions in wall-bounded turbulence at high Reynolds number," Phys. Rev. Fluids **1**, 044405 (2016).

[17] Charitha M de Silva, Dominik Krug, Detlef Lohse, and Ivan Marusic, "Universality of the energy-containing structures in wall-bounded turbulence," J. Fluid Mech. **823**, 498–510 (2017).

[18] W. J. Baars, N. Hutchins, and I. Marusic, "Reynolds number trend of hierarchies and scale interactions in turbulent boundary layers," Phil. Trans. R. Soc. Lond. **375** (2017), 10.1098/rsta.2016.0077.

[19] Charitha M de Silva, Jimmy Philip, Nicholas Hutchins, and Ivan Marusic, "Interfaces of uniform momentum zones in turbulent boundary layers," J. Fluid Mech. **820**, 451–478 (2017).

[20] Ludwig Prandtl, "Zur turbulenten strömung in rohren und längs platten," Ergeb. Aerodyn. Versuch., Series **4**, 18–29 (1932).

[21] T von Karman, "Mechanische ähnlichkeit und turbulenz, nach ges," Wiss. Gottingen. Math. Physik. Klasse (1930).

[22] Ivan Marusic, Jason P Monty, Marcus Hultmark, and Alexander J Smits, "On the logarithmic region in wall turbulence," J. Fluid Mech. **716**, R3 (2013).

[23] G I Barenblatt, "Scaling laws for fully developed turbulent shear flows. Part 1. basic hypotheses and analysis," J. Fluid Mech. **248**, 513–520 (1993).

[24] G I Barenblatt and V M Prostokishin, "Scaling laws for fully developed turbulent shear flows. Part 2. processing of experimental data," J. Fluid Mech. **248**, 521–529 (1993).

[25] Albert A Townsend, *The structure of turbulent shear flow* (Cambridge university press, 1980).

[26] Ludwig Prandtl, "The mechanics of viscous fluids," Aerodynamic theory **3**, 208 (1935).

[27] Marcus Hultmark, Margit Vallikivi, S C C Bailey, and A J Smits, "Turbulent pipe flow at extreme Reynolds numbers," Phys. Rev. Lett. **108**, 094501 (2012).

[28] David K Bisset, Julian C R Hunt, and Michael M Rogers, "The turbulent/non-turbulent interface bounding a far wake," J. Fluid Mech. **451**, 383–410 (2002).

[29] Evatt R Hawkes, Obulesu Chatakonda, Hemanth Kolla, Alan R Kerstein, and Jacqueline H Chen, "A petascale direct numerical simulation study of the modelling of flame wrinkling for large-eddy simulations in intense turbulence," Combustion and flame **159**, 2690–2703 (2012).

[30] N Hutchins and Ivan Marusic, "Evidence of very long meandering features in the logarithmic region of turbulent boundary layers," J. Fluid Mech. **579**, 1–28 (2007).

[31] M Guala, S E Hommema, and R J Adrian, "Large-scale and very-large-scale motions in turbulent pipe flow," J. Fluid Mech. **554**, 521–542 (2006).

[32] Y S Kwon, J Philip, C M de Silva, N Hutchins, and J P Monty, "The quiescent core of turbulent channel flow," J. Fluid Mech. **751**, 228–254 (2014).

[33] Ronald J Adrian, Carl D Meinhart, and Christopher D Tomkins, "Vortex organization in the outer region of the turbulent boundary layer," J. Fluid Mech. **422**, 1–54 (2000).

[34] Richard JAM Stevens, Dennice F Gayme, and Charles Meneveau, "Large eddy simulation studies of the effects of alignment and wind farm length," Journal of Renewable and Sustainable Energy **6**, 023105 (2014).

[35] Myoungkyu Lee and Robert D Moser, "Direct numerical simulation of turbulent channel flow up to $Re_\tau \approx 5200$," J. Fluid Mech. **774**, 395–415 (2015).

[36] Romain Mathis, Nicholas Hutchins, and Ivan Marusic, "Large-scale amplitude modulation of the small-scale structures in turbulent boundary layers," J. Fluid Mech. **628**, 311–337 (2009).

[37] I Marusic, R Mathis, and N Hutchins, "Predictive model for wall-bounded turbulent flow," Science **329**, 193–196 (2010).

[38] N Hutchins, Timothy B Nickels, I Marusic, and MS Chong, "Hot-wire spatial resolution issues in wall-bounded turbulence," J. Fluid Mech. **635**, 103–136 (2009).

[39] KM Talluru, R Baidya, N Hutchins, and I Marusic, "Amplitude modulation of all three velocity components in turbulent boundary layers," J. Fluid Mech. **746**, R1 (2014).

[40] T Wei, P Fife, J Klewicki, and P McMurtry, "Properties of the mean momentum balance in turbulent boundary layer, pipe and channel flows," J. Fluid Mech. **522**, 303–327 (2005).

[41] Gregory L Eyink, "Turbulent flow in pipes and channels as cross-stream inverse cascades of vorticity," Phys. Fluids **20**, 125101 (2008).

[42] J Klewicki, P Fife, and T Wei, "On the logarithmic mean profile," J. Fluid Mech. **638**, 73–93 (2009).

[43] B J McKeon and A S Sharma, "A critical-layer framework for turbulent pipe flow," J. Fluid Mech. **658**, 336–382 (2010).

[44] Stephen B Pope, *Turbulent flows* (IOP Publishing, 2001).

[45] Charles Meneveau and KR Sreenivasan, "The multifractal nature of turbulent energy dissipation," J. Fluid Mech. **224**, 429–484 (1991).

[46] Ivan Marusic, B J McKeon, P A Monkewitz, H M Nagib, A J Smits, and K R Sreenivasan, "Wall-bounded turbulent flows at high Reynolds numbers: Recent advances and key issues," Phys. Fluids **22**, 065103 (2010).

[47] Alexander J Smits, Beverley J McKeon, and Ivan Marusic, "High–Reynolds number wall turbulence," Ann. Rev. Fluid Mech. **43**, 353–375 (2011).

[48] Kirill A Kazakov, "The mean velocity profile of near-wall turbulent flow: is there anything in between the logarithmic and power laws?" J. Turbul **17**, 1015–1047 (2016).

[49] Mark V Zagarola and Alexander J Smits, "Mean-flow scaling of turbulent pipe flow," J. Fluid Mech. **373**, 33–79 (1998).

[50] Jonathan F Morrison, B J McKeon, W Jiang, and A J Smits, "Scaling of the streamwise velocity component in turbulent pipe flow," J. Fluid Mech. **508**, 99–131 (2004).

[51] Xiaohua Wu, Parviz Moin, James M Wallace, Jinhie Skarda, Adrián Lozano-Durán, and Jean-Pierre Hickey, "Transitional–turbulent spots and turbulent–turbulent spots in boundary layers," Proc. Nat. Acad. Sci. USA , 201704671 (2017).

[52] MV Zagarola, AE Perry, and AJ Smits, "Log laws or power laws: The scaling in the overlap region," Phys. Fluids **9**, 2094–2100 (1997).

[53] Hassan M Nagib, Kapil A Chauhan, and Peter A Monkewitz, "Approach to an asymptotic state for zero pressure gradient turbulent boundary layers," Philos. Trans. R. Soc. London, Ser. A **365**, 755–770 (2007).

[54] Beverley J Mckeon, J Li, W Jiang, Jonathan F Morrison, and Alexander J Smits, "Further observations on the mean velocity distribution in fully developed pipe flow," J. Fluid Mech. **501**, 135–147 (2004).

[55] Noor Afzal, "Millikan's argument at moderately large Reynolds number," Phys. Fluids **19**, 600–602 (1976).

[56] You Wu, Xi Chen, ZhenSu She, and Fazle Hussain, "Incorporating boundary constraints to predict mean velocities in turbulent channel flow," SCIENCE CHINA Physics, Mechanics & Astronomy , 1–5 (2012).

[57] Peter A Monkewitz, Kapil A Chauhan, and Hassan M Nagib, "Self-consistent high-Reynolds-number asymptotics for zero-pressure-gradient turbulent boundary layers," Phys. Fluids **19**, 115101 (2007).

[58] Peter A Monkewitz, Kapil A Chauhan, and Hassan M Nagib, "Comparison of mean flow similarity laws in zero pressure gradient turbulent boundary layers," Phys. Fluids **20**, 105102 (2008).

[59] J Klewicki, J Philip, I Marusic, K Chauhan, and C Morrill-Winter, "Self-similarity in the inertial region of wall turbulence," Physical Review E **90**, 063015 (2014).

[60] Joe Klewicki, Paul Fife, Tie Wei, and Pat McMurtry, "A physical model of the turbulent boundary layer consonant with mean momentum balance structure," Philos. Trans. R. Soc. London, Ser. A **365**, 823–840 (2007).

[61] J C Klewicki, "Self-similar mean dynamics in turbulent wall flows," J. Fluid Mech. **718**, 596–621 (2013).

[62] Zhenhua Xia, Yipeng Shi, Renkai Hong, Zuoli Xiao, and Shiyi Chen, "Constrained large-eddy simulation of separated flow in a channel with streamwise-periodic constrictions," J. Fluid Mech. **14**, 1–21 (2013).

[63] Zhenhua Xia, Yipeng Shi, and Shiyi Chen, "Direct numerical simulation of turbulent channel flow with spanwise rotation," J. Fluid Mech. **788**, 42–56 (2016).

[64] Kapil Chauhan, Hassan Nagib, and Peter Monkewitz, "Evidence on non-universality of Kármán constant," Progress in Turbulence II **1**, 159–163 (2007).

[65] Hassan M Nagib and Kapil A Chauhan, "Variations of von Kármán coefficient in canonical flows," Phys. Fluids **20**, 101518 (2008).

[66] William Anderson, Julio M Barros, Kenneth T Christensen, and Ankit Awasthi, "Numerical and experimental study of mechanisms responsible for turbulent secondary flows in boundary layer flows over spanwise heterogeneous roughness," J. Fluid Mech. **768**, 316–347 (2015).

[67] William Anderson, "Amplitude modulation of streamwise velocity fluctuations in the roughness sublayer: evidence from large-eddy simulations," J. Fluid Mech. **789**, 567–588 (2016).

[68] MG Giometto, A Christen, C Meneveau, J Fang, M Krafczyk, and MB Parlange, "Spatial characteristics of roughness sublayer mean flow and turbulence over a realistic urban surface," Boundary-Layer Meteorol. **160**, 425–452 (2016).

[69] B J McKeon and AJ Smits, "Static pressure correction in high Reynolds number fully developed turbulent pipe flow," Meas Sci Technol **13**, 1608 (2002).

[70] Juan C Del Alamo, Javier Jiménez, Paulo Zandonade, and Robert D Moser, "Scaling of the energy spectra of turbulent channels," J. Fluid Mech. **500**, 135–144 (2004).

[71] Sergio Hoyas and Javier Jiménez, "Scaling of the velocity fluctuations in turbulent channels up to $\mathrm{Re}_\tau = 2003$," Phys. Fluids **18**, 011702 (2006).

[72] Adrián Lozano-Durán and Javier Jiménez, "Effect of the computational domain on direct simulations of turbulent channels up to $Re_\tau = 4200$," Phys. Fluids **26**, 011702 (2014).

[73] J Graham, K Kanov, X I A Yang, M Lee, N Malaya, C C Lalescu, R Burns, G Eyink, A Szalay, R D Moser, *et al.*, "A web services accessible database of turbulent channel flow and its use for testing a new integral wall model for

les," J. Turbul **17**, 181–215 (2016).

[74] GI Barenblatt, AJ Chorin, and VM Prostokishin, "Scaling laws for fully developed turbulent flow in pipes," Applied Mechanics Reviews **50**, 413–429 (1997).